AGU PUBLICATIONS

JGR

Journal of Geophysical Research: Oceans

RESEARCH ARTICLE

10.1002/2014JC010225

Hydrography and circulation in the Filchner Depression, Weddell Sea, Antarctica

E. Darelius[1], K. Makinson[2], K. Daae[1], I. Fer[1], P. R. Holland[2], and K. W. Nicholls[2]

[1]Geophysical Institute, University of Bergen and Bjerknes Centre for Climate Research, Bergen, Norway, [2]British Antarctic Survey, Natural Environment Research Council, Cambridge, UK

Key Points:
- New detailed CTD and LADCP sections from the Filchner Depression are presented
- Observations and modeling suggest a new circulation scheme for the depression
- The outflow of ISW in the Filchner Depression occurs along its eastern flank

Correspondence to:
E. Darelius,
darelius@gfi.uib.no

Citation:
Darelius, E., K. Makinson, K. Daae, I. Fer, P. R. Holland, and K. W. Nicholls (2014), Hydrography and circulation in the Filchner Depression, Weddell Sea, Antarctica, *J. Geophys. Res. Oceans*, *119*, 5797–5814, doi:10.1002/2014JC010225.

Received 10 JUN 2014
Accepted 11 AUG 2014
Accepted article online 20 AUG 2014
Published online 5 SEP 2014

Abstract Cold and dense ice shelf water (ISW) emerging from the Filchner-Ronne Ice Shelf cavity in the southwestern Weddell Sea flows northward through the Filchner Depression to eventually descend the continental slope and contribute to the formation of bottom water. New ship-born observations of hydrography and currents from Filchner Depression in January 2013 suggest that the northward flow of ISW takes place in a middepth jet along the eastern flank of the depression, thus questioning the traditional view with outflow along the western flank. This interpretation of the data is supported by results from a regional numerical model, which shows that ISW flowing northward along the eastern coast of Berkner Island turns eastward and crosses the depression to its eastern side upon reaching the Filchner ice front. The ice front represents a sudden change in the thickness of the water column and thus a potential vorticity barrier. Transport estimates of northward ISW flux based on observations ranges from 0.2 to 1.0 Sv.

1. Introduction

Cold ice shelf water (ISW) emerging from the Filchner-Ronne Ice Shelf (FRIS) in the southern Weddell Sea (see Figure 1) flows northward through the Filchner Depression and crosses its sill to eventually descend the continental slope and contribute to the formation of Weddell Sea deep and bottom water [*Foldvik et al*., 2004]. These cold, dense water masses leave the Weddell Sea, e.g., through gaps in the South Scotia ridge, and are major contributors to Antarctic Bottom Water (AABW) formation [*Orsi et al*., 1999].

The outflow of ISW—commonly referred to as the Filchner overflow—was discovered in 1977 [*Foldvik et al*., 1985a] and the flux of cold ISW across the sill has been estimated to 1.6±0.5 Sv (1 Sv $\equiv 10^6 m^3\ s^{-1}$) resulting in 4.3±1.4 Sv Weddell Sea Bottom Water [*Foldvik et al*., 2004]. After crossing the Filchner sill, the relatively dense ISW forms a gravity plume that flows westward along the continental slope, partly being steered downslope by two ridges cross cutting the slope [*Darelius and Wåhlin*, 2007]. The outflow has been monitored sporadically since 1977 and continuously since 2009 with a mooring at the sill (S2, see Figure 1) and the data reveal a seasonal signal in the temperature and salinity of the outflowing water. The seasonality is partly caused by admixture of high salinity shelf water (HSSW) from the Berkner Bank [*Darelius et al*., 2014].

HSSW is formed through cooling of modified warm deep water (MWDW) and additional brine rejection from sea ice formation during winter [*Nicholls et al*., 2009] and it enters the FRIS cavity west of the Berkner Island and through the Ronne depression (see Figure 1). The depression of the freezing point with increasing pressure allows the HSSW ($\theta = T_{f,surface}$) which is here in contact with ice at great depth (the grounding line is as deep as 1800 m) to be transformed into potentially supercooled ($\theta < T_{f,surface}$) ISW: it is cooled, as its heat is used to melt ice, and freshened, as it mixes with the fresh melt water. Since a given amount of heat is associated with a given amount of freshwater, the HSSW-ISW transformation will cause the θS-characteristics (S is salinity) of the water to change along a straight line in θS-space; the Gade line [*Gade*, 1979; *Jenkins*, 1999]. The gradient of the Gade line is 2.4–2.8°C depending on the amount of heat conduction into the ice [*Nicholls et al*., 2009]. The source salinity can be found by extrapolating the Gade line to the point where it intersects the surface freezing point. Following this argument, the HSSW precursor to the overflowing ISW has been found to originate at the Berkner Bank, while the ISW resulting from the slighty more saline Ronne HSSW-inflow is too dense to escape across the Filchner sill and is forced to recirculate within the cavity [*Nicholls et al*., 2001].

The Filchner Depression is filled with ISW up to a depth of about 200–300 m [*Carmack and Foster*, 1975], above which is found winter water or, along the coast, eastern shelf water (ESW). The circulation in the

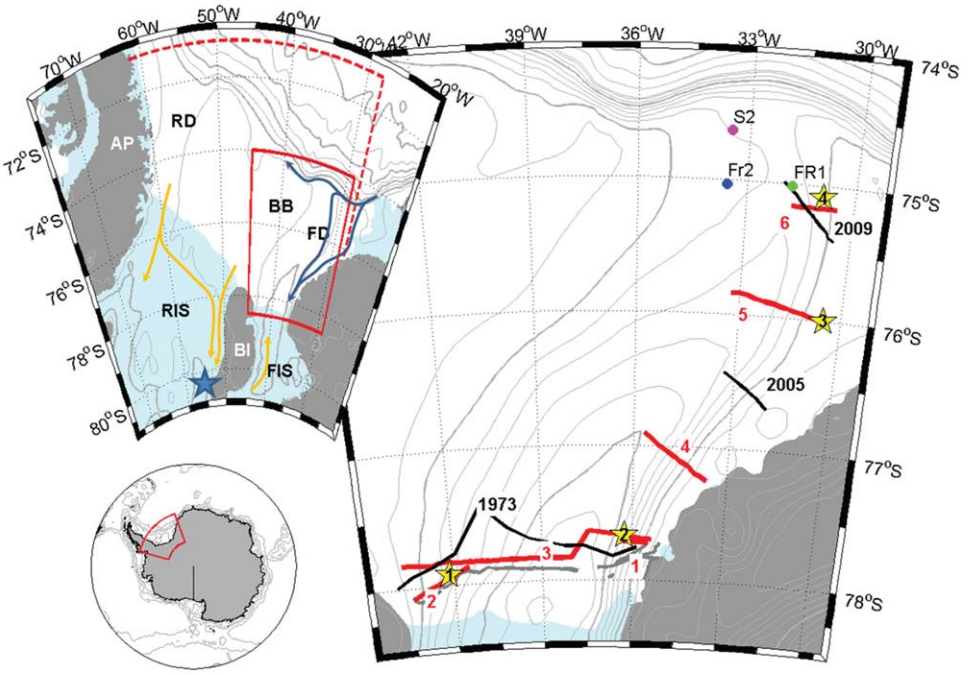

Figure 1. Map of the study region showing the position of the CTD-sections (labeled lines) and time series (labeled yellow stars) occupied in 2013 (red), 2009, 2005, and 1973 (black) and of the moorings Fr1 (green circle), Fr2 (blue circle) and S2 (magenta circle). Isobaths (Bedmap) [*Fretwell et al*., 2013] are shown every 100 m (gray lines) with every 500 m in dark gray. Land and grounded ice is shown in dark gray and floating ice shelves (from Bedmap) in light blue. The position of the ice shelf front (or heavily ridged fast ice in the east) observed during the cruise is included (thin gray line). The upper inset shows the location of the study area (red box) and the Ronne ice shelf (RIS), the Filchner ice shelf (FIS), Berkner Island (BI), Filchner Depression (FD), Ronne depression (RD) and Berkner Bank (BB). The limits of the model domain are indicated by dashed, red lines. The blue arrows show the path of the coastal current/Antarctic slope current and yellow arrows show inflow and circulation below FRIS, from *Nicholls et al*. [2009]. The blue star shows the location of Site 5. The lower inset shows the location of the region (red box) shown in the upper inset.

upper layer in the depression region is described by *Nicholls et al*. [2009] and sketched in the upper inset of Figure 1. Just east of the depression the Antarctic slope current branches off to form a coastal current carrying ESW onto the shelf. Below the surface layer, there is a summer inflow of MWDW toward the ice shelf [*Årthun et al*., 2012], which reaches the Filchner ice front in late summer or early winter [*Foldvik et al*., 1985b; *Årthun et al*., 2013]. While basal melt rates below FRIS are low (0.2–0.34 m yr^{-1}) today [*Nicholls et al*., 2009; *Rignot et al*., 2013], numerical modeling suggest that they will increase significantly (to 4 m yr^{-1}) in a warmer future as changing wind and ice conditions cause more warm water to flow onto the shelf [*Hellmer et al*., 2012]. Based on hydrographic data and geostrophic calculations from the first scientific cruises to the region (USCGC Glacier 1968–1973), *Carmack and Foster* [1975] inferred a cyclonic gyre circulation at depth in the depression. Accordingly, the flow of ISW from the FRIS cavity toward the Filchner sill is commonly believed to follow the topography on the western side of the Filchner Depression [see e.g., *Foldvik and Gammelsrød*, 1988; *Foldvik et al*., 2001; *Nicholls et al*., 2001] although there are no direct observations of the flow as the western part of the depression is often ice-covered even during summer. In this paper, we present detailed sections of hydrography and velocity obtained during a cruise to the Filchner Depression in January 2013 that question the traditional view of the circulation within the depression, and suggest that the core of the ISW outflow is located above the eastern flank of the depression. The observations are compared to results from a regional numerical model, which supports our interpretation of the data.

2. Data and Methods

Data were collected in the Filchner Depression during ten days, 1–11 January 2013, onboard *RRS Ernest Shackleton*. The obtained data set includes vertical profiles of hydrography and velocity from 116 casts with a conductivity-temperature-depth (CTD, SBE911+) package equipped with down and upward-looking lowered acoustic Doppler current profilers (LADCPs, 300 kHz RD Instruments Workhorse). Stations were

Table 1. Information on CTD/LADCP Sections and Time Series Occupied During Cruise ES060, 2013[a]

Stations		Start	End	Time (UTC)	Duration (h)	Angle B (°)	Sta_T
Section 1	6–10	77°43′S, 35°28′W	77°43′S, 36°19′W	3/1 01:30	5	28	
Section 2	12–21	78°05′S, 43°25′W	77°52′S, 41°28′W	3/1 20:40	9	28	
Section 3	29–61	77°50′S, 43°43′W	77°42′S, 35°23′W	5/1 3:50	43	28	
Section 4	70–80	77°15′S, 33°40′W	76°54′S, 35°39′W	7/1 20:50	12	37	73–78
Section 5	90–102	75°59′S, 30°42′W	75°50′S, 33°15′W	9/1 9:10	12	25	93–97
Section 6	103–109	75°50′S, 33°15′W	75°10′S, 31°44′W	10/1 3:50	6	0	105–107
Time Series							
TS1	23–28	77°52′S, 41°28′W		4/1 13:40	10	28	
TS2	62–69	77°40′S, 36°16′W		7/1 02:00	13	28	
TS3	81–89	75°60′S, 30°30′W		8/1 17:30	13	25	
TS4	110–116	75°05′S, 30°52′W		10/1 13:10	12	0	

[a]For location of the sections and time series, see Figure 1. β is the angle that the coordinate system is rotated to be aligned with the slope and Sta_T ares the stations included in the transport estimate (see section 3.2.1., stations are also marked in Figure 6). Time gives the time the first stations in the section/time series was occupied and dates are given in the format day/month.

occupied along six sections: one along the Filchner ice front, one on the western and four on the eastern flank of the depression, and in addition time series (12–14 h long) were obtained at four locations, see Figure 1. The CTD was equipped with double conductivity and temperature sensors and a single oxygen sensor (not shown) which were calibrated by the manufacturer directly after the cruise. In addition, water samples for monitoring of the conductivity sensor were collected using two Niskin bottles attached to the CTD-rosette. The CTD system included an altimeter, allowing for data collection to within 10 m from the bottom. Positions from a Garmin handheld GPS were incorporated directly into the data stream, while data from the positioning system of the ship were recorded separately.

The velocity profiles are calculated at 8 m vertical resolution using the inverse method [*Visbeck*, 2002] constrained by navigation from the GPS and bottom tracking by the LADCP. The error velocity is typically 3 cm s^{-1}. The coordinate system at sections 4–6 and time series 3 and 4 were rotated locally (see Table 1), in order to align the y axis with the isobaths, and velocities are henceforth referred to as along and cross slope. Positive along-slope flow thus has a northeastward direction, i.e., flow toward the sill of the Filchner Depression.

Tides in the region are relatively strong (up to 10–15 cm s^{-1}) and transport calculations based on the LADCP profiles are highly sensitive to errors related to detiding. Attempts were made to detide the LADCP profiles using (1) the tidal model results from the CATS2008b (an update to the circum-Antarctic inverse barotropic tidal model described by *Padman et al*., [2002]), while correcting for errors in the bathymetry of the tidal model using observed depths and conserved volume flux (i.e., $u' = u_{model} h_{model} h_{observed}^{-1}$, where h is the depth and u the tidal current) and (2) harmonic fits to the depth-integrated observed velocities (i.e., volume flux per unit width) at sections and time series, see Appendix A. Observations from the upper and lower 150 m of the profiles were neglected to remove boundary layer effects, as were stations with strong currents above the slope. It is not obvious to draw a conclusion regarding what detiding routine is more correct, see further discussion in Appendix A, and transport estimates are therefore given as an interval spanning the results given by the different detiding procedures. Velocity sections shown in Figures 2, 5, and 7 are detided using CATS.

In addition to the CTD and LADCP data collected during the cruise, sections obtained in the depression in 2005 (JR97) [*Nicholls et al*., 2009] and 2009 (ES033) [*Nicholls*, 2009], at the Filchner ice front in 1973 (USCGC Glacier) [*Carmack and Foster*, 1975] and single stations from 1977 [*Foldvik et al*., 1985a], 1980 [*Foldvik et al*., 1985c], 1984, 1993 [*Gammelsrød et al*., 1994], 1995 [*Grosfeld et al*., 2001], and one station from 2011 (JR244) [*Larter*, 2011] are included in the analysis. Records from ~500 m depth at moorings Fr1 and Fr2 [*Foldvik et al*., 2004] deployed south of the sill in 1995–1996 (see Figure 1 for location) are also included. The data from 1973 have low (10–100 m) vertical resolution.

The transports are calculated using the detided along-slope component of the current velocity. The sections are divided into segments centered at each station and the width of each segment corresponds to half the distance from adjacent stations. For the first and last station segments, the width is set equal to either side of the station. The −1.9°C isotherm is taken as the upper boundary for the ISW in transport calculations. To

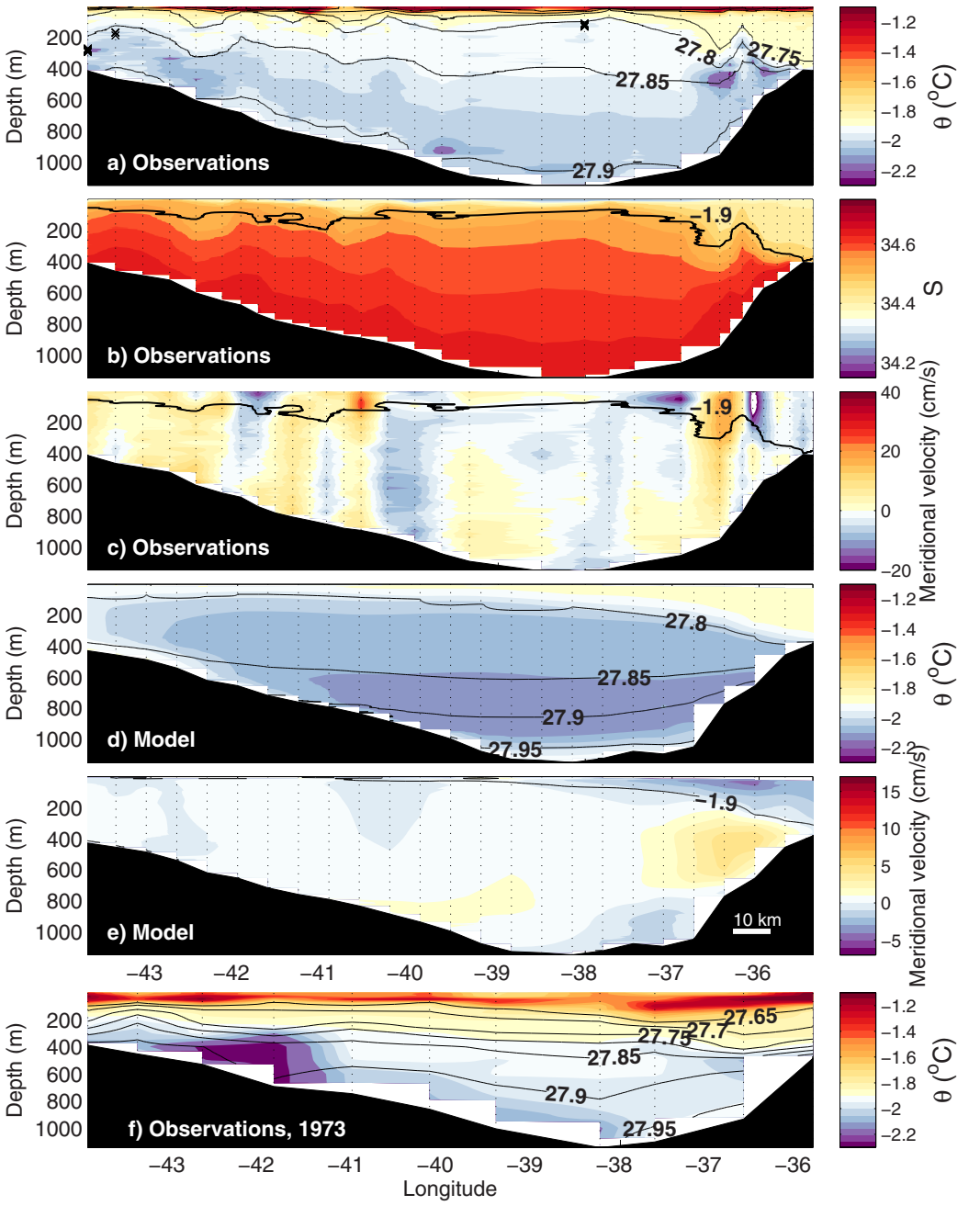

Figure 2. Sections of (a) Potential temperature (color) and isopycnals (labeled black lines) referenced to surface pressure, (b) salinity, and (c) meridional velocity (cm s^{-1}) observed in January 2013 across the Filchner Ice Front (section 3). Mean, modeled sections of (d) potential temperature (color) and isopycnals (labeled black lines) and (e) meridional velocity at 78°S. Section of (f) Potential temperature (color) and isopycnals (labeled black lines) referenced to surface pressure observed in February 1973 [*Carmack and Foster*, 1975]. Observations of in situ supercooled water are marked with black crosses in Figure 2a. The horizontal length scale is shown in the lower right corner of Figure 2e.

limit the error introduced by erroneous detiding, only stations with a baroclinic northward flow are included. The stations included in the transport calculations are given in Table 1 and marked in Figure 5.

The geostrophic shear is calculated using the dynamic height anomaly approach in the Gibbs Seawater Oceanographic Toolbox [*McDougall and Barker*, 2011]. Data from the upper 25 m at each station were ignored to remove surface effects and errors, i.e., the reference level of no motion was effectively set to 25 m. Given the uncertainty in detiding of the LADCP (see Appendix A), absolute geostrophic currents were not calculated. The method gives profiles of relative velocity only above the depth of the shallowest of the two CTD stations used to obtain the profile. In a section across a sloping bottom the geostrophic transport

in what is often referred to as the "bottom triangle," i.e., the area closest to the bottom, is not included unless profiles are somehow extrapolated. This has not been done and transport in the bottom triangle is hence ignored.

The observations are compared with results from an isopycnic coordinate ocean circulation model (MICOM) [*Bleck et al*., 1992] applied to a region including the FRIS cavity and the Filchner Depression (see Figure 1) and adapted to include a thermodynamically active but static ice shelf as well as tidal forcing [*Holland and Jenkins*, 2001]. Following *Jenkins et al*. [2004] the model is forced by restoring the surface salinity over the open ocean to an annually repeating seasonally and spatially varying field [*Makinson et al*., 2011] which is designed to represent the effect of sea ice growth and decay. With the largest tides around Antarctica found in the southern Weddell Sea, the model is also forced along its northern and eastern boundaries by restoring the surface elevations to those predicted by the CircumAntarctic Tidal Simulation (CATS) [*Padman et al*., 2002] utilizing 10 tidal constituents. In the vertical, the model consists of 15 isopycnic layers and a surface mixed layer (with a freely evolving density) while the horizontal resolution increases from 12.5 km in the north to 4.5 km in the south. Explicit vertical mixing in the model occurs through mixed-layer entrainment or detrainment, see *Holland and Jenkins* [2001] for details. After a 13 years spin up, seven years of model data are available as monthly mean fields. The data fields are interpolated to depth coordinates and averaged to a time mean field. The seasonality in the modeled ISW circulation is small and results including only summer months are similar. For further details on the model setup the reader is referred to *Makinson et al*. [2011].

3. Results

3.1. The Filchner Ice Front

3.1.1. Observations

Section 3 was occupied along the entire Filchner ice front at a distance of about 6–30 km from the ice front. Fast ice on the eastern side of the depression forced the ship to move farther north to finish the section. Potentially supercooled ISW is found at depth across the entire Filchner Depression. On the eastern side of the depression, the ISW resides below 300–400 m depth, separated from the ESW above it through relatively sharp gradients in both salinity and temperature (Figures 2a and 2b). The eastern flank is further characterized by low temperatures (down to -2.2°C) in a distinct layer between 350 and 600 m depth. On the western side of the depression, vertical gradients—with the exception of the surface thermo and halocline located at about 50 m depth—are much weaker, and there is little trace of ESW. The internal Rossby radius, $\lambda = (g\Delta\rho h)^{1/2}(\rho_0 f)^{-1}$, where g is gravity, $\Delta\rho = 0.1$ kg m^{-3} the density difference between ESW and the ambient water, h=100–300 m the thickness of the ESW layer and f the Coriolis factor, is about 2–4 km. A coastal current carrying ESW westward along the ice front would hence be trapped south of section 3, since the stations were occupied $>$6 km from the ice front. As discussed below, the ice front section from 1973 which was occupied 1–3 km from the ice front (A. Foldvik, personal communication, 2014) does show a 300–400 m thick layer of ESW below a thin layer of surface water.

Unlike the two stations occupied at the ice front in 1993 [*Gammelsrød et al*., 1994; *Nicholls et al*., 2001] the ISW observed in 2013 does not in general fall on one Gade line, but appears to be a layered mixture of ISW with different source salinities, see e.g., station 32 in Figure 3a. While the larger part of the water column can be expected to have source salinities between 34.68 and 34.70, there are a few cold intrusions (e.g., on station 45, see Figure 3a) indicating higher source salinities. Below the temperature minimum, there is a tendency for stations on the eastern side of the depression to be shifted about 0.05°C downward in θS-space compared to the western stations (i.e., for the same salinity water is 0.05°C colder in the east than in the west). This corresponds to an increase in source salinity of about 0.02.

The lowest temperatures are typically observed 100–300 m above the bottom, and bottom temperatures are generally lower (by about 0.1°C) on the eastern side than on the western side of the depression (Figure 2a). The ISW is by definition potentially supercooled, i.e., its temperature is below the surface freezing point $\theta(z) < T_f(S, 0)$. In a few locations on the western flank of the depression, especially in section 2 (not shown) we also observed water that was *in situ* supercooled (i.e., $T(z) < T_f(S, z)$, Figure 2a). These locations are characterized by upward doming isotherms and low temperatures in the surface but they do not necessarily coincide with locations of flow directed away from the cavity. No *in situ* supercooled water was observed on the eastern flank, possibly because the fast ice forced us to place stations further away from the ice front. *In situ* supercooled ISW in the vicinity of an ice front have been observed previously by e.g., *Fer et al*. [2012].

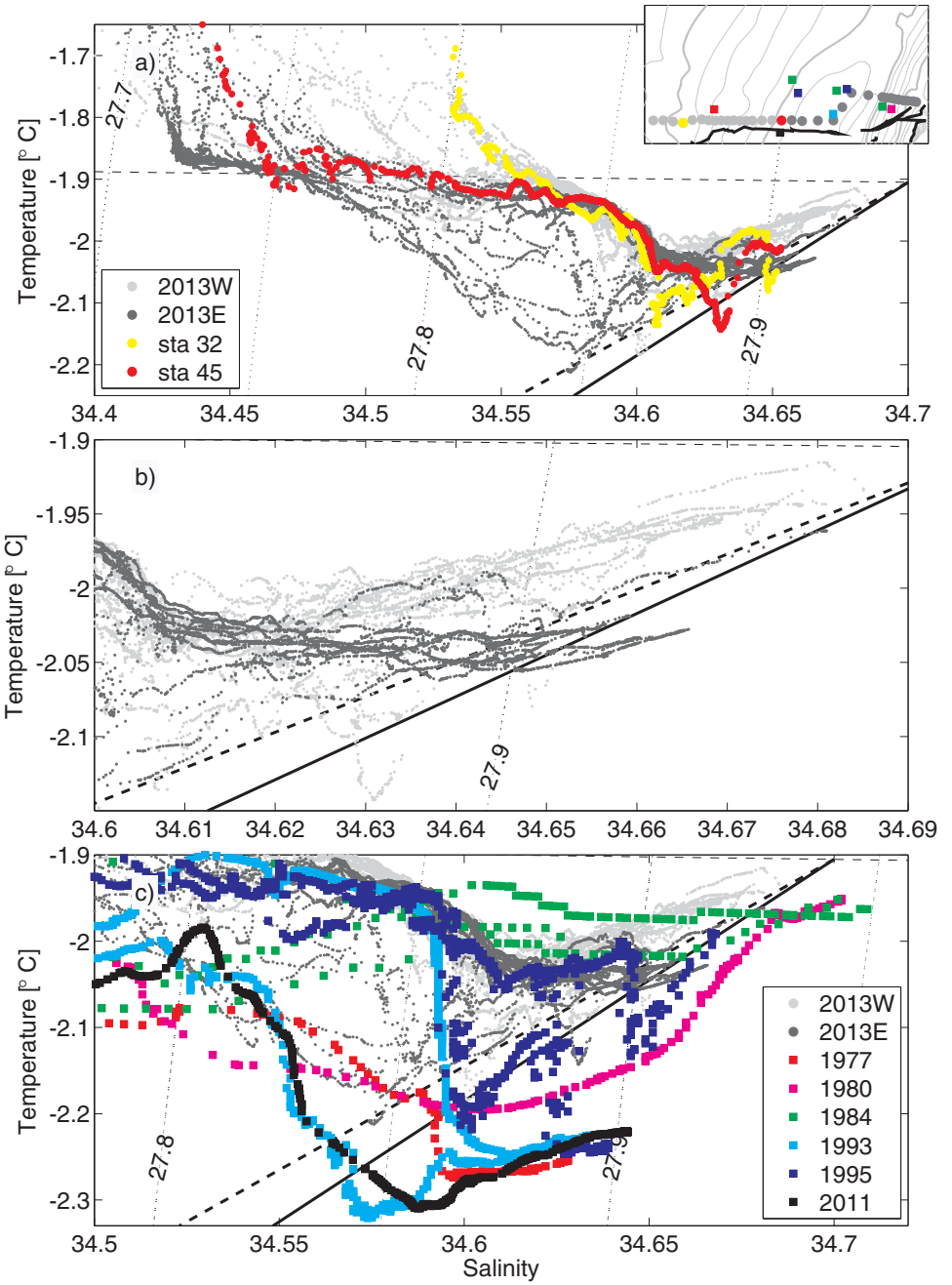

Figure 3. θS-diagram showing (a) data from the Filchner Front in 2013 (section 3) where "eastern" stations are colored dark gray and "western" stations light gray, (b) the same data but zoomed in on the ISW, and (c) selected historic stations occupied in the vicinity of the front according to legend. Dotted, labeled lines are isopycnals referenced to surface pressure, the thin, dashed line is the surface freezing point and thick black lines are Gade lines with a gradient of 2.4 (dashed) and 2.8°C. The inset shows the location of the stations occupied in 2013 (circles) and the historical stations (squares), colored according to the legends in Figures 3a and 3c.

The velocity field at the front is characterized by high variability with lateral length scales of about 10 km and amplitudes reaching 20 cm s^{-1} (Figure 2c), possibly related to instabilities or meanders in a potential (but unobserved) coastal current. Ignoring these mesoscale features, which can be expected to vary in time and space, we note that isopycnals generally are bowl-shaped below about 27.85 kg m^{-3}, while shallower isopycnals deepens from west to east, especially above the eastern flank, i.e., below the southward flowing ESW. The shape of the isopycnals along the ice front indicate a weak (relative geostrophic velocities on the order of a few cm s^{-1}) cyclonic circulation of the densest water in the depression, as suggested by *Carmack*

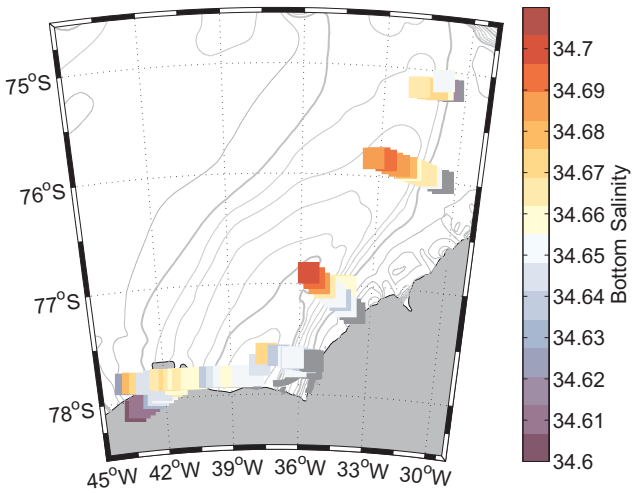

Figure 4. Map showing the bottom salinity at all CTD-stations occupied during cruise ES060, 2013. Stations with a bottom salinity lower than 34.6 are colored equally gray.

and Foster [1975]. On the eastern flank, there is the potential for a northward undercurrent below the southward coastal current, which, if present, would be shadowed by the strong mesoscale variability.

3.1.2. Numerical Model

The modeled ice front section (78°S, Figures 2d and 2e), with the exception of the mesoscale variability, shows features similar to the observations. The depression is filled with ISW up to 50–100 m, with a deepening of the thermocline on the eastern side due to the presence of the southward flowing coastal current and ESW. The isopycnals show the same bowl shape as the observations at depth, and the same eastward deepening at shallower depth. The associated velocity field manifests the deep cyclonic circulation, i.e., outflow on the western flank and inflow on the eastern flank, as identified by *Carmack and Foster* [1975], and supports the idea of a northward flowing undercurrent on the eastern flank as suggested by the tilting isopycnals in the observations. Mean velocities are on the order of a few cm s^{-1} giving a total northward transport of 1.0 Sv, about 0.2 Sv of which returns southward within the deep cyclonic circulation. The model thus has a net northward flow of ISW of 0.8 Sv.

3.1.3. Comparison With USCGC Glacier Section From 1973

The observations warrant a closer comparison with e.g., the ice front section obtained by *USCGC Glacier* in 1973 [*Carmack and Foster*, 1975, Figure 4]. Comparing Figure 2f with Figures 2a and 2b, one notes the following:

(A) The lowest temperatures were observed on the western side in 1973 (and in 1980, 1995) [*Foldvik et al*., 1985c; *Grosfeld et al*., 2001] and on the eastern side in 2013 (and in 1993) [*Gammelsrød et al*., 1994].

(B) Densities below 400 m were higher in 1973 than in 2013. The 27.90 kg m^{-3} isopycnal was found at around 500 m depth in 1973 while it is generally about 50 m above bottom in 2013. No densities above 27.95 were observed in 2013.

(C) The density at sill depth (600 m) was 27.90 kg m^{-3} in 1973 and 27.85 kg m^{-3}, i.e., about 0.05 kg m^{-3} lighter less dense in 2013.

Differences in the upper layer—e.g., the density and the upper limit of the ISW—are most likely related to seasonality and to differences in the distance between the section and the ice front and possibly also to the shape of the ice front itself, which was pointed in 1973 (the stations shown in Figure 1 follows the position of the ice front) while it was relatively straight in 2013.

The comparison suggests changes in the Filchner Depression hydrography that would directly influence the properties of the ISW flowing over the sill and ultimately the deep water masses formed. Figure 3c shows data collected from stations occupied in the vicinity of the Filchner ice front during the period 1977–2013, suggesting that the changes are the result of interannual variability rather than a long-term trend. Large changes in the FRIS-circulation linked to the southern annular mode (SAM) and HSSW production on the Berkner Bank have been suggested by *Timmermann et al*. [2002] for example, and observations from the ice shelf cavity show interannual variability [*Nicholls and Østerhus*, 2004].

Figure 4 shows the bottom salinity observed in 2013. The highest bottom salinities—reaching up to 34.71—were observed at the deepest stations at 76–77°S (sections 4 and 5). At the ice front (sections 1–3) bottom salinities were generally lower with the highest values occurring in the deep, central part of the

depression and at relatively shallow (400–700 m) depths on the western flank of the depression, adjacent to Berkner Bank. The large difference between section 2 and section 3 on the western flank of the depression suggests high temporal and/or spatial variability here. Extrapolating the HSSW-ISW mixing line from stations at the eastern flank (sections 4–6) to the surface freezing point gives a HSSW salinity of 34.72 (Figure 6b), while the western stations in section 3 suggest slightly less saline HSSW.

The observations are consistent with those presented by [*Carmack and Foster*, 1975] and with HSSW formed on Berkner Bank entering the depression and circulating cyclonically along its rim, but not yet having reached the ice front. Observations in 1995 show HSSW presence at the eastern side of the ice front [*Grosfeld et al*., 2001].

3.2. Sections on the Eastern Flank

3.2.1. Observations: Section 4–6

Figure 5 shows the observed hydrography and currents at sections 4–6 on the eastern flank of the depression. The Filchner Depression is filled with ISW up to 100–300 m depth, with the interface depth generally being shallower toward the south. There are clear intrusions of MWDW ($\theta > -1.7$ °C, S $<$34.6) [*Foster and Carmack*, 1976] at section 6, which are found at shelf-level (400–500 m) in the east and at shallower levels—above the ISW—in the depression. The MWDW signal at section 5 is similar but weaker, and at section 4 there is no trace of MWDW. The MWDW intrusions and the erosion of its properties between sections 5 and 6 are evident in θS-space (Figure 6a). Focusing on the ISW, the stations can be divided into two main groups: an eastern group where the θS-relation aligns with a Gade line (slope 2.4) with a source salinity of 34.70 for 34.64 $<$S $<$34.68 and a western group where temperatures in the same salinity range are about 0.05°C higher (Figures 6b and 6c). In addition, there exist a number of "mixed" stations, with "eastern" water at the bottom and "western" water above. The "eastern" and "western" water correspond to water found in the east and the west at the Filchner ice front (Figure 6b). For salinities above 34.68, and more so on the deeper western stations, the θS-relation deviates from the Gade line suggesting admixture of HSSW [*Nøst and Østerhus*, 1998] with a salinity of about 34.72 (Figure 6b).

As observed in the eastern part of section 3 at the ice shelf front, the depth of the densest isopycnals ($\sigma > 27.85$ kg m^{-3}) in section 4–6 generally increase westward, while the depth of the lighter isopycnals decrease westward. The steeply sloping isopycnals at middepth are associated with a relatively strong—maximum observed velocities are 30–40 cm s^{-1}—outflow of ISW located near the 600 m isobath (see Figure 5). The northward transport of ISW above the slope is estimated from the detided LADCP data to be 0.3–0.9, 0.6–1.0, and 0.2–0.3 Sv at section 4–6 respectively. On the shallow shelf in the east, the currents are generally weak with southward flow of ESW and warmer MWDW along the bottom. Currents in section 5 suggest a surface intensified eddy toward the center of the depression (32.25–33°W). Sections 4 and 5 show relatively strong (5–10 cm s^{-1}) barotropic currents with northward flow above the slope and southward flow in the western part of the section and consequently a large barotropic shear. The direction of the flow agrees with the phase of the tidal currents at the time of occupation and are potentially related to tides (see discussion and alternative detiding procedures in Appendix A). Figures 5g–5i show the relative geostrophic currents estimated from the observed hydrography and the thermal wind equation. The strong (up to 20 cm s^{-1}), northward baroclinic current above the slope agrees well with the shear in the observed absolute currents. The baroclinic transport of ISW over the eastern flank of the depression estimated from the geostrophic shear is 0.4, 0.6 and 0.3 Sv at sections 4–6 respectively.

3.2.2. Observations: Sections From 2005 and 2009

Hydrographic sections across the eastern flank of the Filchner Depression have also been occupied in 2005 and 2009 (Figure 7, see Figure 1 for location). They show similar characteristics as the sections discussed above: (A) The depression is filled with ISW up to about 300 m depth, (B) The depth of the shallow isopycnals ($\sigma <$27.85 kg m^{-3}) tilt upward away from the slope while dense isopycnals tilt downward, and (C) MWDW is found at a depth around 350 m in the east and above the ISW, around 250 m depth, in the depression. In addition, the detided LADCP section from 2009, shows an outflow above the 550 m isobath at about 30.9°W.

3.3. Circulation in the Model

Figure 8 shows the modeled mean velocity across three sections: one in the cavity, south of the ice front, one north of the ice front (roughly corresponding to section 3 in ES060) and one perpendicular to the ice

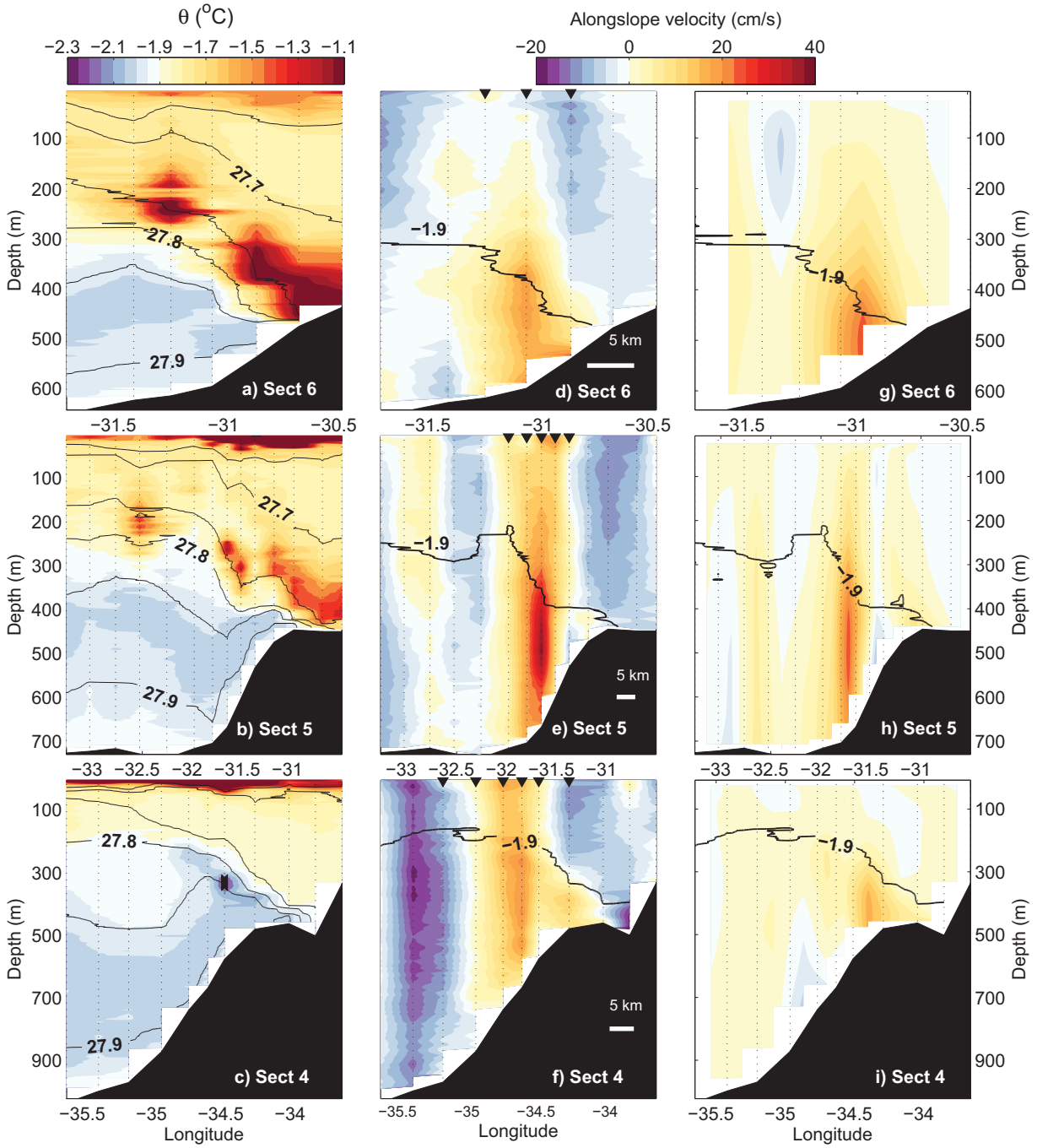

Figure 5. (a–c) Potential temperature (color) and isopycnals (labeled, black lines) referenced to surface pressure, (d–f) along-slope velocity (cm s^{-1}) observed with LADCP in January 2013, and (g–i) Geostrophic shear currents relative to the surface calculated from the observed hydrography. (a, d, g) section 6, (b, e, h) section 5, and (c, f, i) section 4. See Figure 1 for location. Black triangles in Figures 5d–5f mark stations included in ISW transport estimates. The white bar in the lower right corner of Figures 5d–5f is 5 km long. The vertical, dashed lines mark the position of the stations.

front (see inset in Figure 9 for location). Within the cavity at 78.5°S (Figure 8a) approximately 0.9 Sv of ISW flows northward toward the ice front along the eastern side of Berkner Island while there is a weaker 0.3 Sv inflow on the eastern side of the cavity. The core of the northward flow is located between the 27.85 and the 27.90 kg m^3 isopycnal with velocities on the order of 5 cm s^1, while the core of the inflow is slightly denser. North of the ice front (Figure 8b), the core of the northward flow has shifted to the eastern side of the depression, where it is centered between the 27.80 and the 27.85 kg m^3 isopycnal, beneath the southward flowing

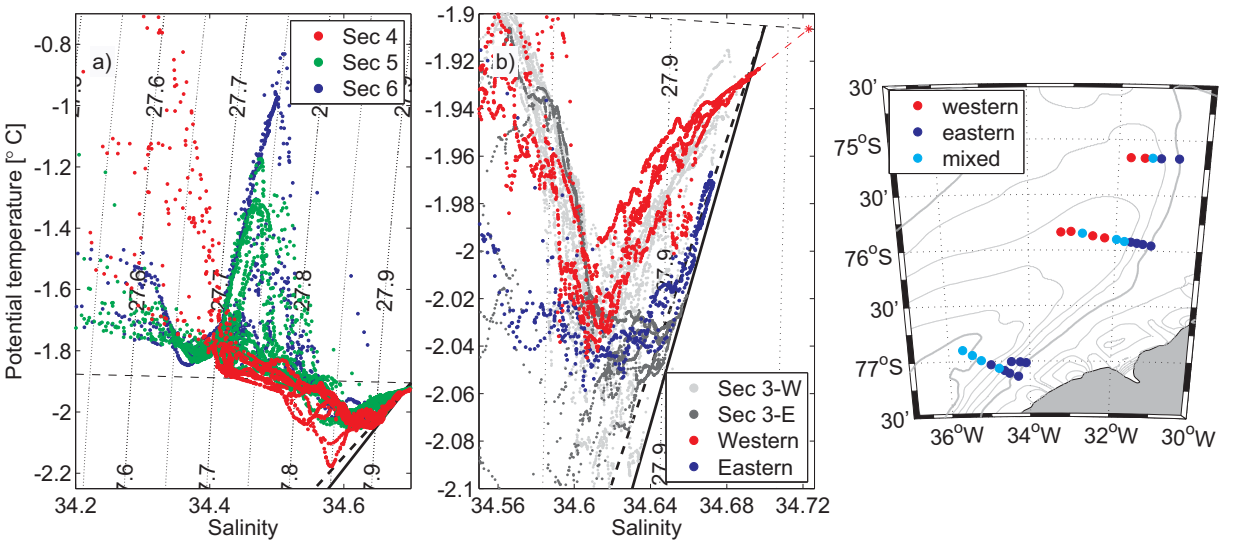

Figure 6. θS-diagram showing data from (a) the eastern flank of the depression in 2013 (sections 4–6) and (b) 76°S (section 5) and stations from the Filchner Front (section 3). For location of sections, see Figure 1. Note the different scales in Figures 6a and 6b. Dotted, labeled lines are isopycnals referenced to surface pressure, the thin, dashed line is the surface freezing point and thick black lines are Gade lines with a gradient of 2.4 (dashed) and 2.8°C. The red, dashed line shows the extrapolation of the ISW-HSSW mixing line and the red star indicates the inferred properties of the HSSW. (c) Map showing the location of stations in Figure 6a where the color of the dot indicates if the station can be characterized as "eastern," "western," or "mixed" (see text and Figure 6b).

coastal current and over a denser southward undercurrent. Apart from the relatively strong currents in the east, there is a general slow northward motion across the larger part of the depression.

The section normal to the ice front (Figure 8c) shows a relatively narrow zone of high shear separating the westward flowing coastal current from an eastward flowing core of ISW that resides just south of the ice front. By the time the shallower coastal current reaches 39.9°W, its density has been changed significantly through mixing along the length of the ice front and no longer has ESW characteristics. The eastward flow of ISW is located just south of the ice front and extends from the ice shelf base at about 500 m down to 900 m depth.

The transport across the sections shown in Figure 8, divided in density classes, is shown in Figure 9. We note that (A) the density of the northward flowing water has significantly decreased between the two zonal sections (78.5°S and 77.9°S), suggesting intensive mixing at the ice front (B) north of the ice front, the northward transport on the eastern and western side is of roughly equal magnitude (Figure 9b) (C) northward flowing ISW with densities equal to the main northward flow observed in the cavity (27.90 kg m^3, 78.5°S) are observed mainly on the western side of the depression (77.9°S west) suggesting minimal mixing as it crosses this part of the ice front, (D) the fresher and lighter ESW ($<$ 27.77 kg m^3) in the coastal current, which is prominent in eastern part of the section north of the ice front (77.9°S east), has disappeared in the section perpendicular to the ice front (39.9°W) as a result of the intense mixing along the ice front, (E) the deep southward flow has a slightly greater density resulting from the input of HSSW originating from Berkner Bank, and (F) the southward flow at 78.5°S south of the ice front, which does not include any ESW, is roughly two times larger than the southward transport north of the ice front (77.9°S) meaning that about half of the recirculating water remains within a cyclonic gyre that straddles the ice front.

North of the ice front, the middepth outflow of ISW flows northward, gathering into a focused current that occupies the water column from about 300 m to 600 m depth along the eastern flank of the depression until reaching the Filchner Sill. The modeled velocity field agrees well with the mean currents observed at mooring Fr1–2 and explains why, contrary to what was expected from the traditional circulation scheme, no northward flow was observed at Fr2 (Figure 10).

3.4. Potential Vorticity and Ice Front Dynamics

The draft of the ice shelf is about 400–600 m at the ice front [*Lambrecht et al.*, 2007], and compared to the total water depth of up to 1200 m the ice front represents a large step in the thickness of the water column (H) and a discontinuity in the fH^{-1} contours (Figure 11a), suggesting that the ice front constitutes a

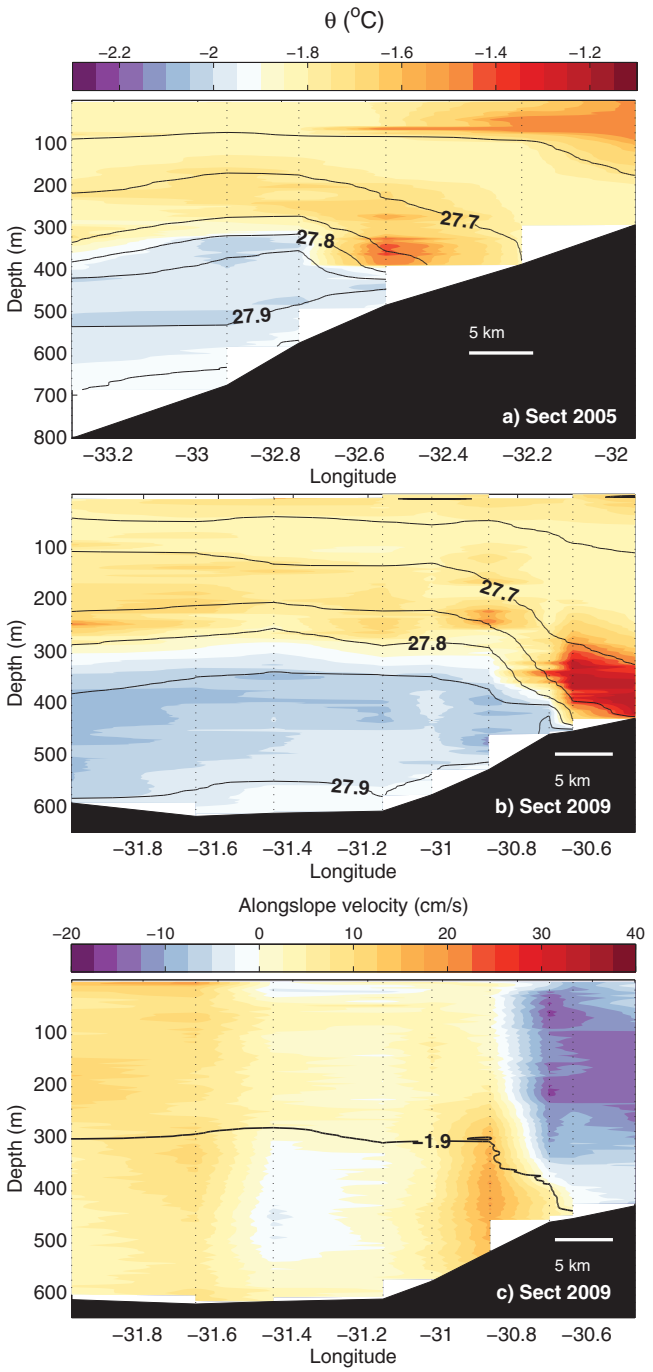

Figure 7. Sections of potential temperature (color) and isopycnals (labeled, black lines) referenced to surface pressure from sections across the eastern flank in (a) 2005 and (b) 2009. (c) Along-slope velocity (cm s^{-1}) observed in 2009. The upper limit of ISW (given as the −1.9°C isotherm) is marked with a thin, black line in Figure 7c. The horizontal white bar in the lower right corner of each subplot is 5 km long.

potential vorticity (PV) barrier. The components of the Ertel potential vorticity [*Pedlosky*, 1986] were calculated using the mean velocity and density fields while neglecting the vertical velocity component. The PV field is dominated by the planetary stretching term, slightly modified at the ice front by the relative vorticity term while the tilting term is negligible. A simpler expression for the PV, $((\rho_2-\rho_1)\rho_0^{-1}fH_\rho^{-1}$, where H_ρ is the thickness of the layer delimited by the ρ_1 and ρ_2 isopycnals) also gives a PV-field similar to that depicted in Figure 11b, which shows the Ertel PV-field at the 27.87 kg m^{-3} isopycnal, which is within the density class with maximum eastward flow at 39.9°W. A region with constant Ertel PV extends along the eastern side of Berkner Island, bifurcating at the ice front with one branch crossing the ice front along the western flank (i.e., no cross ice front gradient in Ertel PV) and the other branch extending eastward, running parallel to the ice front. Along the eastern part of the ice front, where the core of the northward flow is observed, there is a strong cross ice front Ertel PV gradient.

4. Discussion

New, detailed *in situ* observations from the Filchner Depression and results from regional numerical modeling using MICOM suggest a circulation pattern that challenges—or at least complements—previously proposed circulation schemes from the region [*Foldvik and Gammelsrød*, 1988; *Foldvik et al.*, 2001; *Nicholls et al.*, 2001]. A revised circulation pattern is presented in Figure 12. The core of the northward flowing ISW which eventually crosses the Filchner sill and contributes to bottom water formation is found along the *eastern* flank of the depression and not—as previously proposed—along the western flank (Figure 12). Below the outflow, there is a relatively weak cyclonic circulation, as observed by *Carmack and Foster* [1975]. Previous circulation schemes are based on interpretation of very limited data sets in which the relatively narrow current above the eastern flank

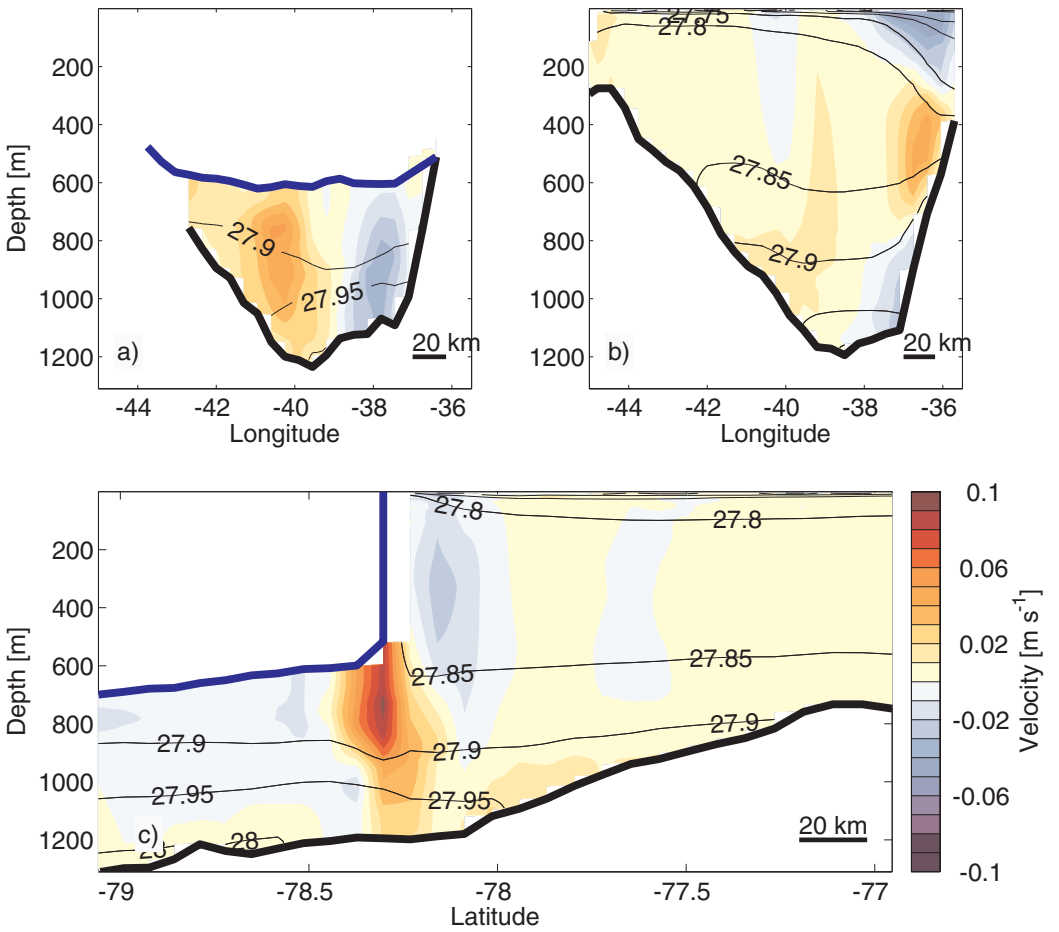

Figure 8. Sections of modeled mean velocity perpendicular to the section at (a) 78.5°S (b) 77.9°S, and (c) 39.9°W. Positive velocities are northward, i.e., in to the paper in Figures 8a and 8b and eastward, i.e., out of the paper in Figure 8c. The position of the sections is shown in the inset in Figure 9. The velocity scale given in Figure 8c is valid for all plots. Labeled, thin, black lines show isopycnals referenced to surface pressure, the thick, black line indicates the bottom and the thick, blue line the draft of the ice shelf. The horizontal, black bar in the lower right corner of each subplot is 20 km long.

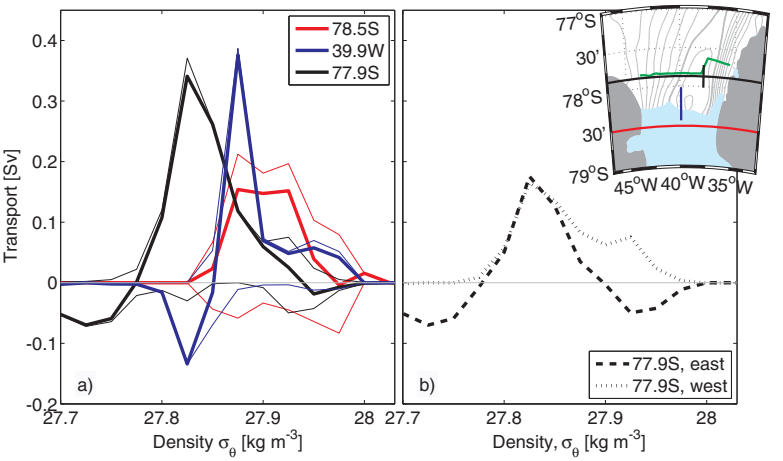

Figure 9. Modeled transport in density classes (a) through sections parallel and perpendicular to the front according to the legend and (b) through the eastern and western part of the section at 77.9°S. Thin lines show total in and outflow and thick lines show net flow. Positive transports are northward for the zonal sections and eastward for the meridional section. The inset in Figure 9b shows the location of the sections, including CTD section 3 from ES060 which is shown in green. The black, vertical line in the middle of section 77.9°S indicates the division between "77.9°S east" and "77.9°S west" shown in Figure 9b.

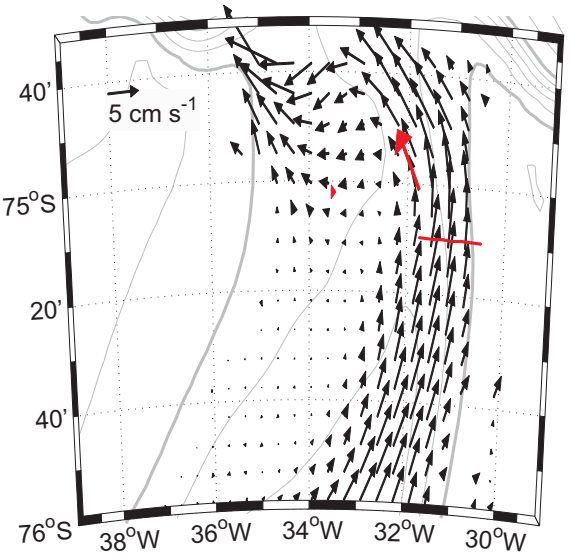

Figure 10. Modeled mean currents at 460 m depth (black lines). The velocity scale is given in the upper left corner. The mean current observed at Fr1 (480 m depth) and Fr2 (450 m depth) [*Foldvik et al.*, 2004] is shown as red arrows and the red line indicates the location of section 6.

was not captured. The revised circulation scheme proposed here results directly from improved station coverage and insight gained from the regional modeling, giving a better understanding of the system, rather than to a change in the physical system itself. The new circulation scheme also agrees well with the existing mooring observations (Fr1–2, Figure 10) and previous hydrographic surveys (Figure 7).

The transport estimates based on the LADCP sections are highly sensitive to the detiding and the uncertainty in the transport estimates are relatively high. Unfortunately, the current data set and the available tidal models do not allow for a better quantification of the transport and current strength. A northward flow along the eastern flank of the depression is however present in all sections from 2013 as well as two sections from 2005 and 2009 and its existence is not compromised by detiding errors. While the difference in transport between sections 4 and 5 is within the error bars, the transport at section 6 near the sill is significantly lower. This might be related to temporal variability, but it is also possible that the section did not capture the entire outflow. As suggested by the modeled currents in Figure 10, the outflow in the vicinity of the sill occurs on both sides of the Depression with comparable magnitude. At the location of section 6 however, the flow in the model is still concentrated on the eastern flank.

The northward flow of ISW is thus occurring on the eastern and not, as previously thought, on the western side of the Depression. This means that the dense water to a higher degree is in contact with lighter ESW, but also with the seasonal inflow of warm MWDW [*Årthun et al.*, 2012] compared to an outflow situated on the western flank of the Depression. The seasonality of the outflow observed at the sill is however not related to the admixture of ESW or MWDW, but to HSSW from the Berkner Bank [*Darelius et al.*, 2014]. While it is beyond the scope of this study, the presence of a northward flow of ISW along the eastern flank is likely to influence the dynamics of the inflow of warm MWDW toward the cavity.

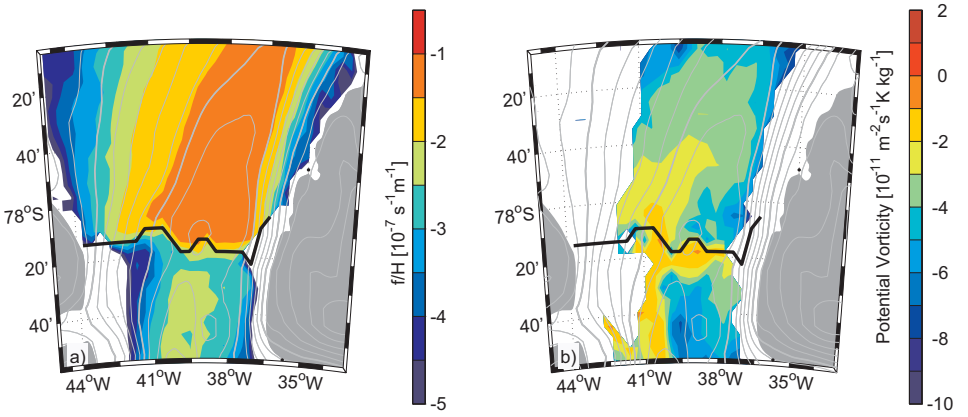

Figure 11. Map showing (a) fH^{-1} contours, where H is the thickness of the water column and (b) mean Ertel potential vorticity at the mean 27.87 kg m^{-3} isopycnal surface. Isobaths are shown every 100 m (gray lines) and the Filchner ice front is indicated in black.

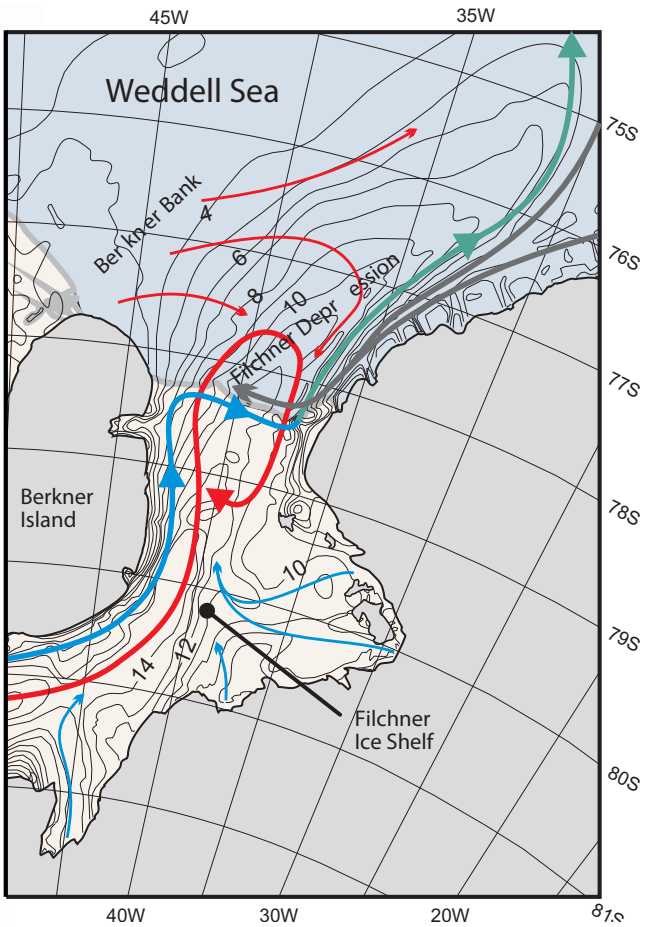

Figure 12. Map showing a schematic of the proposed circulation beneath Filchner Ice Shelf (light gray shading) and within the Filchner Depression. The thick colored arrows beneath the ice shelf show the main circulation originating from the western (red) and eastern (blue) ends of the Ronne Ice Front. The thin colored lines show minor flows of ISW (blue) from deeper ice and HSSW flowing into Filchner Depression from Berkner Bank (red). The coastal currents are shown in dark gray, with main ISW outflow on the eastern flank of Filchner Depression in dark green. Bathymetric contours are labeled in hundreds of meters.

The deep cyclonic circulation can be expected to entrain the HSSW descending into the depression from the Berkner Bank [*Carmack and Foster*, 1975; *Nøst and Østerhus*, 1998] and carry it into the FRIS cavity (as schematically shown by the thin red lines in Figure 12). This is observed in the numerical model. The observations from January 2013 show—much like the observations from 1973—that the bottom salinity north of the ice front (section 4) is higher than the bottom salinity at the ice front, suggesting that a seasonal pulse of HSSW from the Berkner Bank has descended into the Depression but not yet reached the Filchner ice front. The seasonality of the HSSW drainage into the depression is supported by CTD-profiles obtained between 75 and 76°S above the eastern flank of the depression: profiles from February to April 2011 show presence of HSSW while profiles obtained in May–September the same year do not [*Darelius et al*., 2014]. With a length scale of about 200 km and velocities of a few cm s^{-1}, the advective time scale for the flow of HSSW in the Depression would be on the order of 2–7 months. Seasonal pulses of HSSW entering the depression can thus be expected to be "flushed out" before the arrival of next season's HSSW. This is in accordance with the results by *Nøst and Østerhus* [1998] suggesting that the residence time for water in the Filchner Depression is shorter than two years.

Results from the numerical model imply that part of the northward flow of ISW, which follows the western flank of the depression within the cavity, shifts over to the eastern flank while following the Filchner ice front across the depression. The draft of the ice front is about 400–600 m [*Lambrecht et al*., 2007], and compared to a total depth of the depression of about 1000 m, it represents a significant and sudden change in the thickness of the water column. We thus hypothesize—supported by Figure 11—that the behavior of the ISW in the ice front region is governed by vorticity dynamics, and that part of the ISW is unable to cross the step in topography but is forced to follow the ice front eastward. The situation is to a large extent analogue (but up-side down) to a coastal current encountering a sudden change in bathymetry—an escarpment—upon which it bifurcates in two branches, one leaves the coast to flow parallel to the escarpment and the other continues along the coast [see e.g., *Carnevale et al*., 1999; *Cenedese*, 2005]. The ice front has previously been suggested to act as a PV-barrier to HSSW inflow [see e.g., *Grosfeld et al*., 1997]. A region of constant Ertel PV (Figure 11b) extends northward along the eastern side of Berkner Island and divides in two: one part continuing northward along the western flank of the depression, one part flowing eastward

parallel to the ice front. It was shown in Figure 9 that water leaving the ice shelf cavity along the eastern flank of the depression is exposed to intensive mixing at the ice front (since the density of the northward flow north of the ice front is reduced compared to the flow within the cavity) and the Ertel PV signal is lost. The absence of a continuous Ertel PV-field across the ice front does not mean that water is not crossing the ice front. On the western side of the depression Ertel PV-contours cross the ice front, and the model results show northward flow of unmodified cavity water (i.e., water north of the ice front has similar density and Ertel PV as water within the cavity).

The observations suggest that the depression in 2013 was filled with ISW having variable source salinities and Figure 3 suggests even larger variability in source salinity on interannual timescales. For example, the very cold ISW observed at the ice front in 2011—which suggests source salinities of 34.75 – is not seen in 2013, when source salinities are lower (34.68−34.7) and temperatures higher. The large differences between 2011 and 2013 support the finding by *Nøst and Østerhus* [1998] that the residence time of the ISW in the Filchner Depression is shorter than two years. Differences in source salinities can be due to either (A) spatially variable sources, i.e., a shift from source water originating from Berkner Bank to water originating from the Ronne Depression and/or (B) temporal variability of source waters from one location, due either to seasonal or interannual changes in ice production and preconditioning. It seems likely that the small variability observed between and at stations in 2013 is due to (B), especially when taking into account that the ISW emanates from several different deep, high melt, locations (and thus different paths and residence times) of melt below FRIS [*Holland et al*., 2007; *Makinson et al*., 2011] while the larger interannual variability e.g., between 2011 and 2013 would be caused by (A). CTD-profiles obtained through access holes drilled southwest of Berkner Island (Site 5, see large inset in Figure 1) in 1999 [*Nicholls et al*., 2001] show a two layered structure with high (34.77) source salinity ISW at the bottom and lower source salinity (S=34.66) water at the top. The high source salinity water originates from the Ronne Depression [*Nicholls et al*., 2001] and corresponds to the ISW found in the Filchner Depression in 1977, 1993, and 2011 while the low salinity source water originates from the Berkner Bank and corresponds more closely to the ISW filling the depression, e.g., in 2013 and partly in 1995. Interestingly, the two stations occupied at the western side of the ice front in 1995 show Ronne source water, while the two western stations are dominated by ISW originating at the Berkner Bank [*Grosfeld et al*., 2001] suggesting an ongoing transition from Ronne source water, which dominated the water column in 1993, to Berkner source water, which dominated the Filchner outflow in 1998 [*Nicholls et al*., 2001]. The changes observed in the Filchner Depression suggest a reorganization of the circulation beneath FRIS, which is likely to be linked to atmospheric forcing as proposed e.g., by *Timmermann et al*. [2002], but its origin and the mechanisms involved is beyond the scope of this study. Changes in the circulation beneath FRIS can be expected to influence the circulation in the depression, and consequently the volume flux and properties of the Filchner overflow and the bottom waters generated.

Appendix A: Detiding of LADCP Velocity Profiles

Tidal currents in the Filchner region are relatively strong (10–15 cm s^{-1}) and transport estimates based on LADCP velocity profiles are highly sensitive to errors in detiding. Attempts were made to detide the LADCP profiles using (1) the tidal model results from the CATS2008b (an update to the circum-Antarctic inverse barotropic tidal model described by *Padman et al*. [2002]) and (2) harmonic fits to the depth-integrated

Table A1. Northward Transport of ISW Across Sections 4–6 Calculated Using Different Detiding Procedures

		ISW flux (Sv)		
	Detiding	Section 4	Section 5	Section 6
1	CATS2008b	0.9	1.0	0.3
2a	Time series[a]		0.7	
2b	Time series + Section, excluding stations with strong currents[b]		0.9	
2c	Time series + Section, excluding stations with very strong currents[b]		0.6	
2d	Section, excluding stations with strong currents[c]	0.7		0.3
2e	Section, excluding stations with very strong currents[c]	0.3		0.2

[a]Including constituents M2, M4, S2.
[b]Including constituents M2/S2/M4/K1/O1.
[c]Including constituents M2.

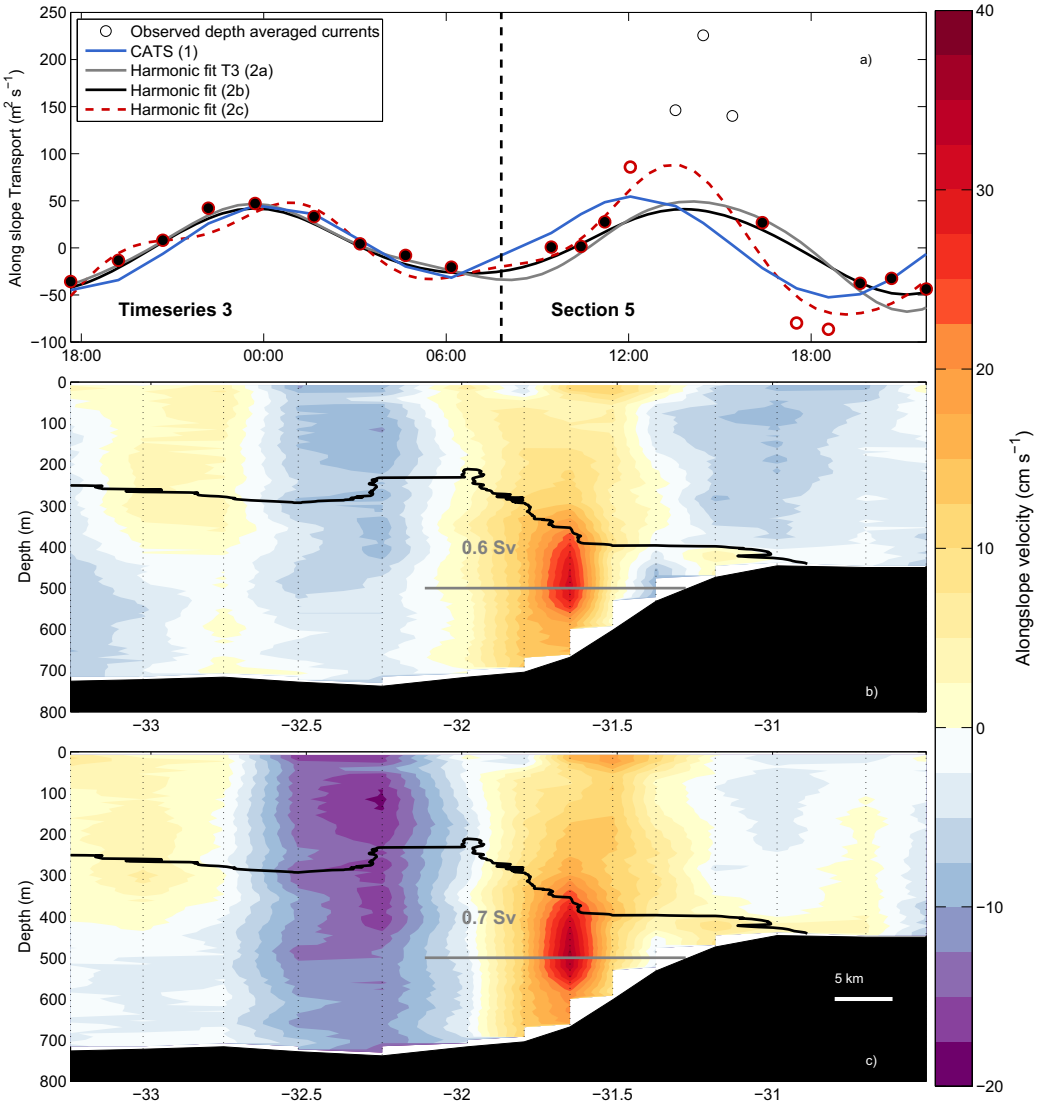

Figure A1. (a) Observed, depth integrated along-slope current (circles; stations included in 2b are colored black, stations included in 2c have red border) from time series 3 and section 5 (see Figure 1 for location) and tidal predictions from tidal model (blue line) and harmonic fits to stations from T3 (2a: gray line) and section 5 + T3 (2b: black line, 2c dashed red line). The dashed black line marks the end of T3. Observed along-slope current at section 5 detided using harmonic fit Figure A1b) 2a (gray line in Figures A1a and A1c) 2c (dashed red line in Figure A1a). The gray lines in Figure A1b and A1c marks the stations included in the transport estimate and the number gives the along slope transport of ISW. The horizontal white bar in the lower right corner of Figures A1b and A1c is 5 km long and the black line is the −1.9°C isotherm.

observed fluxes. Observations from the upper and lower 150 m of the profiles were neglected to remove boundary layer effects, as were stations with strong currents above the slope. Harmonic analysis were carried out including stations from time series and/or sections (see Table A1). Figure A1 shows the observed depth integrated fluxes and tidal predictions from TS3 and section 5, which were occupied consecutively, and two examples of detided currents.

In general, predictions from the tidal model (CATS2008b) agree well with the time series, especially for TS 1 and 3 where the rms error is <1.5 cm s^{-1}. However, when predictions from the tidal model were applied to the sections, or when the harmonic fits derived from the time series are extrapolated and used to detide a nearby section, the residual depth integrated currents are relatively strong (up to 10 cm s^{-1}) above the slope and in the deeper part of the depression. The currents are in phase with the tides, suggesting that tidal currents here are stronger than predicted by the model. When combining stations from the time series and the nearby section in harmonic analysis, the tidal predictions for the time series appear less good

(Figure A1a). The occupation of sections 4 and 5 are "in phase" with each other: it took roughly 12 h to occupy the sections (Table 1) and tidal currents were directed northward above the slope and southward in the deeper part of the depression during the occupation of both sections.

Estimates of northward transport across sections 4–6 were calculated as outlined in section 2 using the different detiding procedures and the results are presented in Table A1. Transport estimates in section 3 are given as an interval using the lower and upper transport estimate from Table A1. Figures presented in section 3 are detided using the tidal model.

Acknowledgments

The authors are grateful to A. Wåhlin and Göteborg University, Sweden for kindly providing CTD, Rosette and sensors, to T. Aspen, M. Reigstad and J. T. Eiliertsen at University of Tromsø, Norway for kindly providing the CTD-winch during cruise ES060 in 2013 and to C. Chavanne for sharing his Matlab routines for tidal calculations. Assistance during cruise ES060 from the crew of RRS Ernest Shackleton, H. Bryhni, K. Vaage and M. Jensen was much appreciated. This work was carried out under the project WEDDELL with funding from the Norwegian Research Council, and the study is also part of the British Antarctic Survey Polar Science for Planet Earth Programme funded by The Natural Environment Research Council. Data availability: Model results, data from cruise ES060 and older data from Norwegian cruises are available from the authors upon request while data from cruise ES033, JR97 and JR244 are available at www.bodc.ac.uk and observations from 1973 at www.nodc.noaa.gov/OC5/WOD13.

References

Årthun, M., K. W. Nicholls, K. Makinson, M. A. Fedak and L. Boehme (2012), Seasonal inflow of warm water onto the southern Weddell Sea continental shelf, Antarctica, *Geophys. Res. Lett.*, *39*, L17601, doi:10.1029/2012GL052856.

Årthun, M., K. W. Nicholls, and L. Boehme (2013), Wintertime water mass modification near an Antarctic Ice Front, *J. Phys. Oceanogr.*, *43*(2), 359–365, doi:10.1175/JPO-D-12-0186.1.

Bleck, R., C. Rooth, D. Hu, and L. T. Smith (1992), Salinity-driven thermocline transients in a wind-and thermohaline-forced isopycnic coordinate model of the North Atlantic, *J. Phys. Oceanogr.*, *22*, 1486–1505, doi:10.1175/1520-0485(1992)022¡1486:SDTTIA2.0.CO;2.

Carmack, E. C., and T. D. Foster (1975), Circulation and distribution of oceanographic properties near the Filchner Ice Shelf, *Deep Sea Res. Oceanogr. Abstr.*, *22*(2), 77–90, doi:10.1016/0011-7471(75)90097-2.

Carnevale, G., S. G. L. Smith, F. Crisciani, R. Purini, and R. Serravall (1999), Bifurcation of a coastal current at an escarpment, *J. Phys. Oceanogr.*, *29*, 969–985.

Cenedese, A. (2005), Effects of a topographic gradient on coastal current dynamics, *J. Geophys. Res.*, *110*, C09009, doi:10.1029/2004JC002632.

Darelius, E., and A. Wåhlin (2007), Downward flow of dense water leaning on a submarine ridge, *Deep Sea Res., Part I*, *54*(7), 1173–1188, doi:10.1016/j.dsr.2007.04.007.

Darelius, E., K. O. Strand, S. Østerhus, T. Gammelsrød, M. Årthun and I. Fer (2014), On the seasonal signal of the Filchner Overflow, Weddell Sea, Antarctica, *J. Phys. Oceanogr.*, *44*, 1230–1243, doi:10.1175/JPO-D-13-0180.1.

Fer, I., K. Makinson, and K. W. Nicholls (2012), Observations of thermohaline convection adjacent to Brunt Ice Shelf, *J. Phys. Oceanogr.*, *42*(3), 502–508, doi:10.1175/JPO-D-11-0211.1.

Foldvik, A., and T. Gammelsrød (1988), Notes on Southern Ocean hydrography, sea-ice and bottom water formation, *Palaeogeogr. Palaeoclimatol. Palaeoecol.*, *67*, 3–17.

Foldvik, A., T. Gammelsrød, and T. Tørresen (1985a), Hydrographic observations from the Weddell Sea during the Norwegian Antarctic research expedition 1976/77, *Polar Res.*, *3*, 177–193.

Foldvik, A., T. Gammelsrød, and T. Tørresen (1985b), Circulation and water masses on the southern Weddell Sea shelf, in *Oceanology of the Antarctic Continental Shelf, Antarct. Res. Ser.*, vol. 43, edited by S. S. Jacobs, pp. 5–20, AGU, Washington, D. C.

Foldvik, A., T. Gammelsrød, and T. Tørresen (1985c), Oceanographic conditions on the Weddell Sea shelf during the German Antarctic Expedition 1979/80, *Polar Res.*, *3*, 195–207.

Foldvik, A., T. Gammelsrød, E. Nygaard, and S. Østerhus (2001), Current measurements near Ronne Ice Shelf: Implications for circulation and melting, *J. Geophys. Res.*, *106*(C3), 4463–4477, doi:10.1029/2000JC000217.

Foldvik, A., T. Gammelsrød, S. Østerhus, E. Fahrbach, G. Rohardt, M. Schröder, K. W. Nicholls, L. Padman and R. A. Woodgate (2004), Ice shelf water overflow and bottom water formation in the southern Weddell Sea, *J. Geophys. Res.*, *109*, C02015, doi:10.1029/2003JC002008.

Foster, T. D., and E. C. Carmack (1976), Frontal zone mixing and Antarctic Bottom Water formation in the Southern Weddell Sea, *Deep Sea Res. Oceanogr. Abstr.*, *23*, 301–317.

Fretwell, P., et al. (2013), Bedmap2: Improved ice bed, surface and thickness datasets for Antarctica, *Cryosphere*, *7*(1), 375–393, doi:10.5194/tc-7-375-2013.

Gade, H. (1979), Melting of ice in sea water: A primitive model with application to the Antarctic ice shelf and icebergs, *J. Phys. Oceanogr.*, *9*(1), 189–198.

Gammelsrød, T., A. Foldvik, O. A. Nøst, Ø. Skagseth, L. Anderson, E. Fogelqvist, K. Olsson, T. Tanhua, E. Jones, and S. Østerhus (1994), Distribution of water masses on the continental shelf in the southern Weddell Sea, in *The Polar Oceans and Their Role in Shaping the Global Environment, Geophys. Monogr. Ser.*, vol. 85, edited by O. M. Johannessen, R. D. Muench, and J. E. Overland, pp. 159–176, AGU, Washington, D. C.

Grosfeld, K., R. Gerdes, and J. Determann (1997), Thermohaline circulation and interaction between ice shelf cavities and the adjacent open ocean, *J. Geophys. Res.*, *102*(C7), 15,595–15,610, doi:10.1029/97JC00891.

Grosfeld, K., M. Schröder, E. Fahrbach, R. Gerdes, and A. Mackensen (2001), How iceberg calving and grounding change the circulation and hydrography in the Filchner Ice Shelf-Ocean system, *J. Geophys. Res.*, *106*(C5), 9039–9055.

Hellmer, H. H., F. Kauker, R. Timmermann, J. Determann, and J. Rae (2012), Twenty-first-century warming of a large Antarctic ice-shelf cavity by a redirected coastal current., *Nature*, *485*(7397), 225–228, doi:10.1038/nature11064.

Holland, D., and A. Jenkins (2001), Adaptation of an isopycnic coordinate ocean model for the study of circulation beneath ice shelves, *Mon. Weather Rev.*, *129*, 1905–1927.

Holland, P. R., D. L. Feltham, and A. Jenkins (2007), Ice Shelf Water plume flow beneath Filchner-Ronne Ice Shelf, Antarctica, *J. Geophys. Res.*, *112*, C05044, doi:10.1029/2006JC003915.

Jenkins, A. (1999), The impact of melting ice on ocean waters, *J. Phys. Oceanogr.*, *29*(3), 2370–2381.

Jenkins, A., D. M. Holland, K. W. Nicholls, M. Schröder, and S. Østerhus (2004), Seasonal ventilation of the cavity beneath Filchner-Ronne Ice Shelf simulated with an isopycnic coordinate ocean model, *J. Geophys. Res.*, *109*, C01024, doi:10.1029/2001JC001086.

Lambrecht, A., H. Sandhäger, D. G. Vaughan, C. Mayer (2007), New ice thickness maps of FilchnerRonne Ice Shelf, Antarctica, with specific focus on grounding lines and marine ice, *Antarct. Sci.*, *19*, 521–532, doi:10.1017/S0954102007000661.

Larter, R. D. (2011), Cruise report RRS James Clark Ross JR244, Marine geoscience and physical oceanography, southern Weddell Sea and South Orkney continental shelf, January-March 2011, technical report number JR244, British Antarctic Survey, Cambridge, U. K.

Makinson, K., P. R. Holland, A. Jenkins, K. W. Nicholls, and D. M. Holland (2011), Influence of tides on melting and freezing beneath Filchner-Ronne Ice Shelf, Antarctica, *Geophys. Res. Lett.*, *38*, L06601, doi:10.1029/2010GL046462.

McDougall, T. J., and P. M. Barker (2011), *Getting Started With TEOS-10 and the Gibbs Seawater (GSW) Oceanographic Toolbox*, 28pp., SCOR/IAPSO WG127, S-10.org.

Nicholls, K., S. Østerhus, K. Makinson and M. Johnson (2001), Oceanographic conditions south of Berkner Island, beneath FilchnerRonne Ice Shelf, Antarctica, *J. Geophys. Res.*, *106*(C6), 11,481–11,492.

Nicholls, K. W. (2009), Cruise report RRS Ernest Shackleton ES033, Second ACES-FOCAS cruise to the southern Weddell Sea 22 January-7 March 2009, technical report, ES033, Br. Antarct. Surv., Cambridge.

Nicholls, K. W., and S. Østerhus (2004), Interannual variability and ventilation timescales in the ocean cavity beneath Filchner-Ronne Ice Shelf, Antarctica, *J. Geophys. Res.*, *109*, C04014, doi:10.1029/2003JC002149.

Nicholls, K. W., S. Østerhus, K. Makinson, T. Gammelsrød and E. Fahrbach (2009), Ice-ocean processes over the continental shelf of the southern Weddell Sea, Antarctica: A review, *Rev. Geophys.*, *47*, RG3003, doi:10.1029/2007RG000250.

Nøst, O. A. and S. Østerhus (1998), Impact of grounded icebergs on the hydrographic conditions near the Filchner Ice Shelf, in *Ocean, Ice, and Atmosphere—Interaction at the Antarctic Continental Margin*, vol. 75, edited by S. S. Jacobs and R. Weiss, pp. 267–284, AGU, Washington, D. C.

Orsi, A. H. H., G. C. Johnson, and J. L. Bullister (1999), Circulation, mixing, and production of Antarctic Bottom Water, *Prog. Oceanogr.*, *43*(1), 55–109, doi:10.1016/S0079-6611(99)00004-X.

Padman, L., A. Fricker, R. Coleman, S. Howard, and S. Erofeeva (2002), A new tidal model for the Antarctic ice shelves and seas, *Ann. Glaciol.*, *34*, 247–254, doi:10.3189/172756402781817752.

Pedlosky, J. (1986), *Geophysical Fluid Dynamics*, 2nd ed., 710 pp., Springer, N. Y. and Berlin.

Rignot, E., S. Jacobs, J. Mouginot, and B. Scheuchl (2013), Ice-shelf melting around Antarctica, *Science*, *341*(6143), 266–70, doi:10.1126/science.1235798.

Timmermann, R., H. H. Hellmer, and A. Beckmann (2002), Simulations of ice-ocean dynamics in the Weddell Sea 2. Interannual variability 1985–1993, *J. Geophys. Res.*, *107*(C3), 3025, doi:10.1029/2000JC000742.

Visbeck, M. (2002), Deep velocity profiling using lowered acoustic Doppler current profilers: Bottom track and inverse solutions*, *J. Atmos. Oceanic Technol.*, *19*, 794–807.